

10/2-3-95 JSD

Conf-9408125--47

# HIGH GRADIENT TESTS OF SLAC LINEAR COLLIDER ACCELERATOR STRUCTURES\*

J.W. Wang, H. Deruyter, J. Eichner, K.H. Fant, H.A. Hoag, R.F. Koontz, T. Lavine  
G.A. Loew, R. Loewen, L. Menegat, R.H. Miller, C. D. Nantista, C. Pearson  
R.D. Ruth, S.G. Tantawi, A.E. Vlieks, P.B. Wilson, and C. Yoneda  
Stanford Linear Accelerator Center, Stanford University, Stanford, CA 94309, USA

## Abstract

This paper describes the current SLAC R&D program to develop room temperature accelerator structures for the Next Linear Collider (NLC). The structures are designed to operate at 11.4 GHz at an accelerating gradient in the range of 50 to 100 MV/m. In the past year a 26 cm constant-impedance traveling-wave section, a 75 cm constant-impedance traveling-wave section, and a 1.8 m traveling-wave section with detuned deflecting modes have been high-power tested. The paper presents a brief description of the RF test setup, the design and manufacturing details of the structures, and a discussion of test results including field emission, RF processing, dark current spectrum and RF breakdown.

## Experimental Setup

Accelerator structures described in this paper were all tested in the Accelerator Structure Test Area (ASTA) facility located

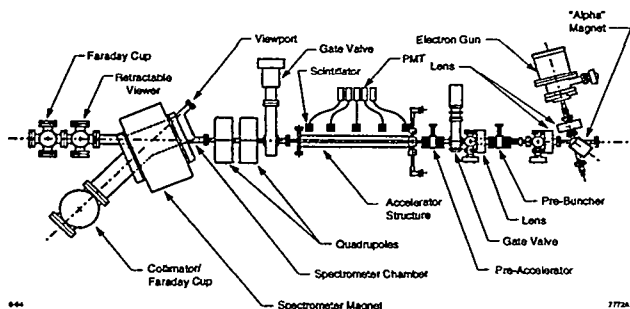


Fig. 1. Layout of the Accelerator Structure Test Area.

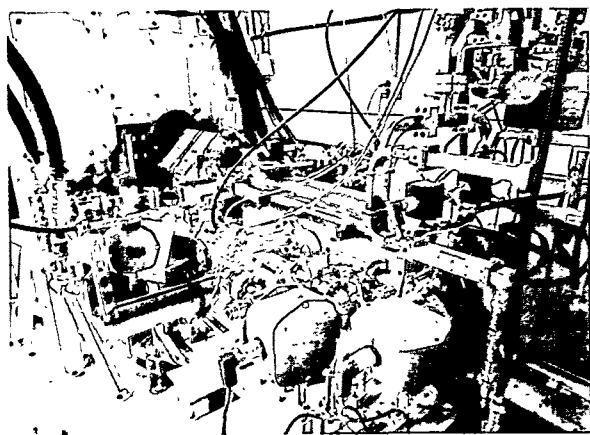


Fig. 2. Experimental setup for high-power tests of the 75 cm traveling-wave section.

\*Work supported by Department of Energy contract DE-AC03-76SF00515

inside a shielded area. As shown in Fig. 1, ASTA consists of a gun and beam focusing system, a prebuncher, a pre-accelerator, a precision rail for mounting the accelerator sections to be tested, and a 45° spectrometer capable of analyzing electron beam energies up to 200 MeV with a resolution of ±0.5%. The accelerator structures are powered by a SLAC X-Band klystron followed by a SLED-II pulse compression system.

## Accelerator Structures

The characteristics and main RF parameters of the traveling-wave (TW) X-Band sections are shown in Table 1. The short (7-cavity) standing-wave (SW) structure is listed here only for reference.

The 26 cm (30-cavity) constant-impedance structure was constructed out of simple self-jigging nesting cups, which were then brazed together. The input end was equipped with a symmetrically fed coupler designed to minimize the phase and amplitude asymmetries in the coupler fields.

The 75 cm (86-cavity) constant-impedance section (see Fig. 2) was a design prototype for longer X-Band structures. Water cooling tubes and parallel vacuum pumping manifolds

TABLE 1  
Characteristics of Tested Structures

Parameter	6 cm (SW)	26 cm (TW)	75 cm (TW)	1.8 m (TW)
Frequency, f (MHz)	11424	11424	11424	11424
Structure type	C.I.	C.I.	C.I.	Detuned
Iris diameter, 2a (cm)	0.75	0.75	0.856	1.134 - 0.786
Cavity diameter, 2b (cm)	2.12	2.12	2.158	2.284 - 2.139
Disk thickness, t (cm)	0.146	0.146	0.146	0.1-0.2
Total cavities	7	30	86	206
Shunt impedance (MΩ/m)	98/2	98	88	67- 88
Factor of merit, Q	6960	6960	7005	7020
Coupler type	Single	Double	Double	Double
Group velocity, v <sub>g</sub> /c	—	0.033	0.048	0.118 - 0.03
Filling time, T <sub>f</sub> (ns)	80	26.5	52	100
Attenuation, τ	—	0.136	0.267	0.505
RF pulse length (ns)	770	60	75	75
Peak input power (MW)	13.8	116	130	105
Maximum E <sub>acc</sub> (MV/m)	—	108†	90†	65†
Average E <sub>acc</sub> (MV/m)	110*	101†	79†	55†
Max. surface, E <sub>s</sub> (MV/m)	500*	235†	206†	131†
E <sub>s</sub> /E <sub>acc</sub>	4.55	2.275	2.292	2.37‡

\* Limited by RF breakdown

† Limited by klystron output power

‡ E<sub>s</sub>/E<sub>acc</sub>

MASTER

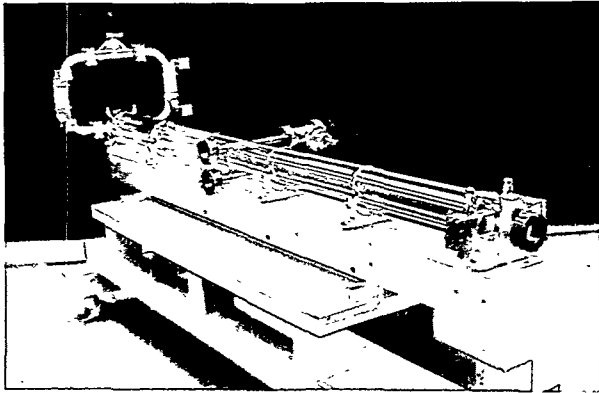


Fig. 3. First 1.8 m detuned accelerator section.

were integrated into each cell. The cells were made by single-point diamond turning to produce optical quality surface finishes, with cavity and iris diameter tolerances of  $\pm 2.5 \mu\text{m}$ .

The 1.8 m (206-cavity) detuned structure (see Fig. 3) is a first model for the NLC Test Accelerator at SLAC. Each cavity has a different diameter, iris diameter, and disk thickness so as to detune the higher-order dipole modes in a Gaussian pattern while keeping a constant  $2\pi/3$  phase shift per cavity for the accelerating mode. Six cavities have radial pumping holes to two outer vacuum manifolds. The manifolds increase the pumping speed by an order of magnitude. This improvement is considered necessary to handle the increased gas load resulting from high peak power operation.

### Experimental Results

The main RF parameters and experimental results for the three traveling-wave X-Band accelerator structures are summarized in Table 1.

The 6 cm and early 26 cm structure test results were reported in a previous paper [1]. After the RF system was

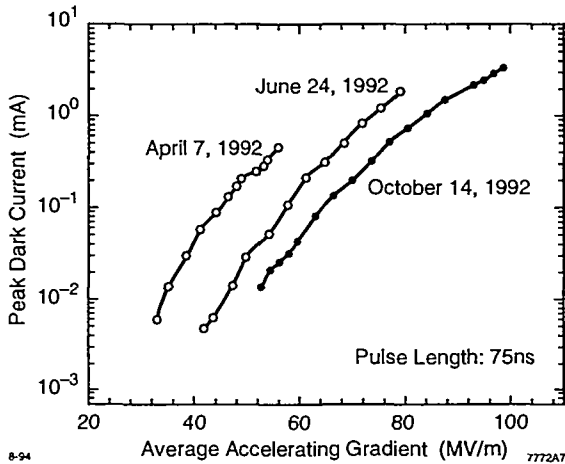


Fig. 4. Peak dark current measured by a downstream Faraday cup for the 26 cm traveling-wave section as a function of average accelerating gradient for three stages of RF processing.

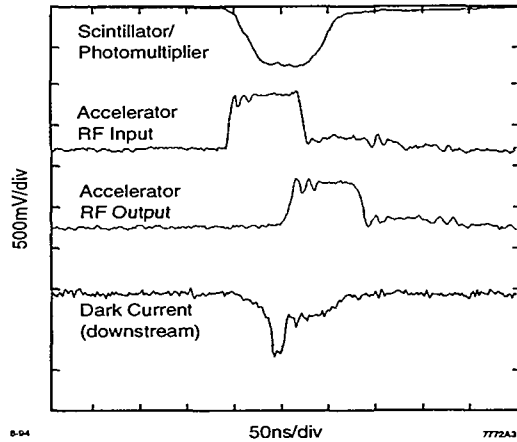


Fig. 5. Scintillator/Photomultiplier output, Input RF pulse, Output RF pulse, and Dark Current Waveforms for the 75 cm traveling-wave section at average accelerating gradient of 80 MV/m.

upgraded, the peak input power for the 26 cm structure was increased from 75 MW to 116 MW. It took 20 hours of RF processing to bring the accelerating gradient at the beginning of the 26 cm structure up to 108 MV/m. This corresponded to an average accelerating gradient of more than 100 MV/m. Figure 4 shows the dark current as a function of average accelerating gradient. The dark current was reduced by a factor of more than 20 after proper RF processing.

Figure 5 shows various oscilloscope traces for the 75 cm TW structure tests. The overshoot in the beginning of the dark current pulse is believed to be caused by more electrons being captured in the first 30 ns of the RF pulse when the higher frequency transient due to the fast rise time results in a lower phase velocity. The scintillator/photomultiplier output pulse gives a fairly good indication of the X-ray intensity caused by

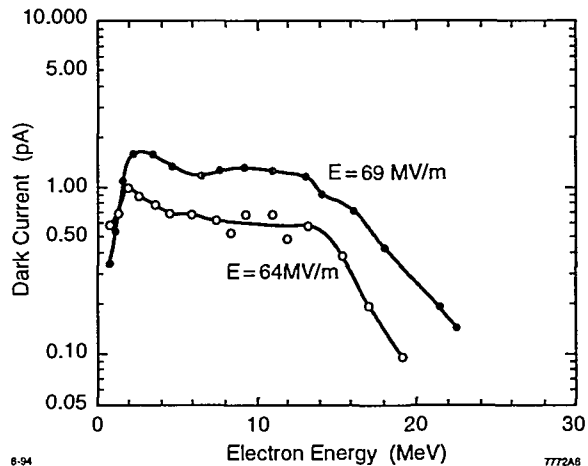


Fig. 6 Average dark current at a fixed spectrometer slit as a function of electron energy for two different gradients in the 75 cm traveling-wave accelerator section.

## DISCLAIMER

This report was prepared as an account of work sponsored by an agency of the United States Government. Neither the United States Government nor any agency thereof, nor any of their employees, makes any warranty, express or implied, or assumes any legal liability or responsibility for the accuracy, completeness, or usefulness of any information, apparatus, product, or process disclosed, or represents that its use would not infringe privately owned rights. Reference herein to any specific commercial product, process, or service by trade name, trademark, manufacturer, or otherwise does not necessarily constitute or imply its endorsement, recommendation, or favoring by the United States Government or any agency thereof. The views and opinions of authors expressed herein do not necessarily state or reflect those of the United States Government or any agency thereof.

## **DISCLAIMER**

**Portions of this document may be illegible in electronic image products. Images are produced from the best available original document.**

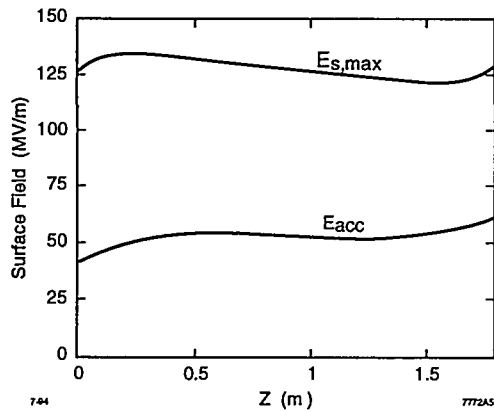


Fig. 7. Calculated peak surface and accelerating gradient along the 1.8 m detuned accelerator section.

bremstrahlung of field emitted electrons. Figure 6 shows the momentum-analyzed average dark current measured for two different gradients with the  $45^\circ$  spectrometer (refer back to Fig. 1). The collimator slit width was set at 5.3 mm. The relatively flat top of the two curves indicates that the dark current was captured fairly uniformly along the structure.

For the 1.8 m detuned structure, the accelerating gradient along the length is shown in Fig. 7. The profile is almost flat like in a conventional constant-gradient structure: the first cavities have a thinner disk, larger iris aperture, and somewhat lower accelerating field; the last cavities have a thicker disk, smaller iris aperture, and somewhat higher accelerating field. The peak surface field on the disk edges varies by less than 5% along the whole structure. Figure 8 is a record of the RF processing: it took 30 hours over a two-day period to reach an average accelerating gradient of 50 MV/m. Figure 9 shows input and output RF waveforms for the two arms of the couplers. For a total peak input of 98 MW and output of

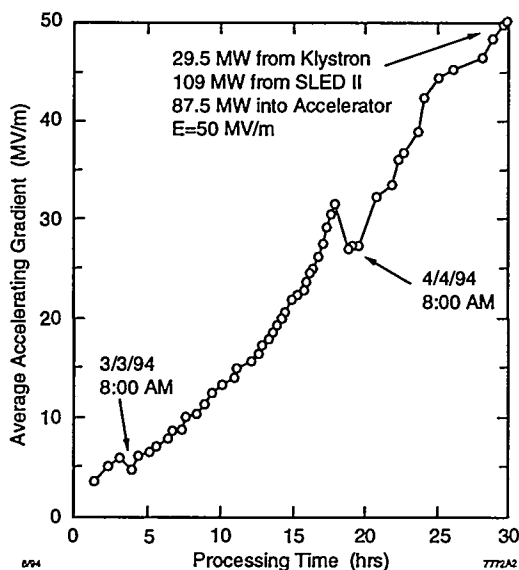


Fig. 8. Radio frequency processing schedule for the 1.8 m detuned accelerator section.

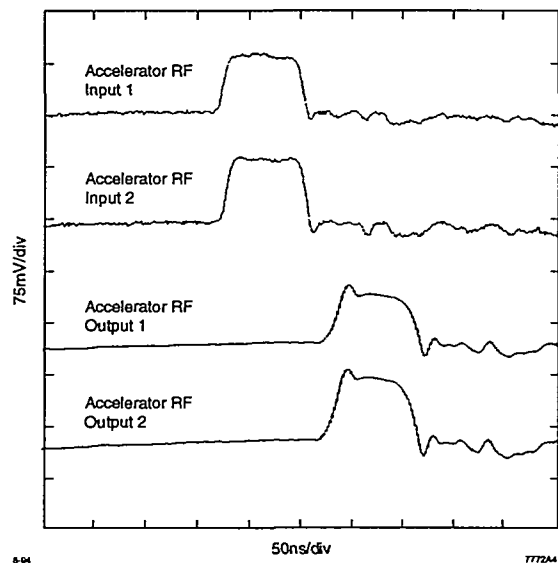


Fig. 9. Input and output RF waveforms for the 1.8 m detuned section at average accelerating gradient of 53 MV/m.

27.6 MW, the average accelerating gradient was 53 MV/m. The dark current as a function of accelerating gradient was plotted in Fig. 10 to be compared with the results for the 75 cm section. Note that there was not enough RF power available to process the 1.8 m structure to even higher gradient. According to our experience [2], the dark current might have been further reduced if the available RF processing power had been higher.

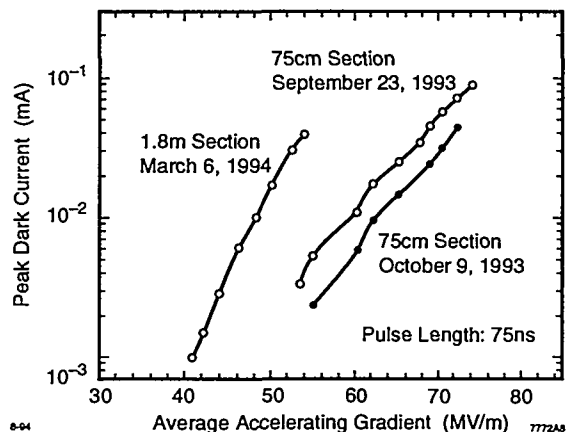


Fig. 10 Peak dark current measured by a downstream Faraday cup for the 75 cm constant-impedance and the 1.8 m detuned section as a function of average accelerating gradient.

### Reference

1. J. W. Wang et al, "High Gradient Studies On 11.4-GHz Copper Accelerator Structures," LINAC 92, Ottawa, Canada, August 1992; SLAC-PUB-5900 (1992).
2. G.A. Loew and J.W. Wang, "RF Breakdown Studies in Room Temperature Electron Linac Structures," (for 13th Int. Symp. on Discharges and Electrical Insulation in Vacuum, Paris, France, 1988), SLAC-PUB-4647 (1988).